Effect of Magnesia Addition on the Densification and Mechanical Properties of Zinc Aluminate Ceramic

Buzhe CUI [1], Jianying HAO [1]*, Zhenguo ZHU [2], Shuo BAI [2], Jianguo WU [1]

[1] *School of Materials Science and Engineering, Taiyuan University of Science and Technology, Taiyuan 030024, China*
[2] *Institute of Metal Research, Chinese Academy of Sciences, Shenyang, 110016, China*

http://doi.org/10.5755/j02.ms.39605

Received 28 November 2024; accepted 2 February 2025

Zinc aluminate ($ZnAl_2O_4$) ceramic has attracted more and more attention because of its superior properties. $ZnAl_2O_4$ ceramic was successfully synthesized via solid-state reaction sintering using alumina and zinc oxide as raw materials and magnesia as an additive. The phase composition and microstructure of sintered samples were characterized by XRD and SEM. The densification of $ZnAl_2O_4$ ceramic containing 2.5 % magnesia is significantly improved, 6.01 % of apparent porosity and 4.1 g/cm^3 of bulk density. Additionally, the flexural strength achieves the maximum of 198.7 MPa, which is 91.2 % higher than that without magnesia addition. During sintering, Mg^{2+} can substitute Zn^{2+} to form $(Mg_xZn_{1-x})Al_2O_4$ spinel, promoting the development and growth of $ZnAl_2O_4$ grains and making the structure denser. The free Zn^{2+} can inhibit grain boundary migration and locally refine grains, resulting in an increase of the strength.
Keywords: zinc aluminate ceramic, mechanical property, densification, magnesia.

1. INTRODUCTION

Zinc aluminate ($ZnAl_2O_4$, ZA) spinel is gaining more and more attention, particularly in the field of refractory. Typically, spinel refractory is classified into two types: traditional alkaline ($MgCr_2O_4$ spinel) and emerging $MgAl_2O_4$ spinel (MA) [1, 2]. Comparing with the potential environmental hazards of $MgCr_2O_4$ and the acid intolerance of MA, ZA exhibits high melting temperature (1950 ℃), regular thermal expansion coefficient (7×10^{-6} ℃$^{-1}$ in the range of 25 ℃ – 900 ℃), high thermal stability and good resistance to acids and alkali. Consequently, ZA has rapidly emerged as the premier choice for refractory materials [3].

The synthesis process of ZA ceramic included solid-state reaction sintering, hot pressing (HP), spark plasma sintering (SPS) and microwave (MW) heating.[4-9] Compared with other methods, solid-state reaction sintering was one of the most preferable processes due to its simple process, low energy consumption and easy popularization for synthesizing high temperature ceramics [4 – 6]. Consequently, the solid-state reaction sintering is the most widely used method in industrial production. Furthermore, the sintering additives and various metal oxide additives have been extensively investigated to improve the properties of ZA ceramic. Studies have shown that these additives effectively inhibit grain growth, accelerate sintering rates and reduce sintering temperatures. Ouyang fabricated ZA ceramic by solid-state reaction sintering using zinc borate as an additive and found that zinc borate could effectively improve the properties of ZA ceramic and expand the sintering temperature range [4]. Qin demonstrated that the sintering temperature of ZA ceramic prepared by solid-state reaction was reduced from 1400 ℃ to 930 ℃ by using Li-Mg-Zn-B-Si glass as a sintering aid [5]. Belyaev synthesized ZA ceramic by hot pressing (1600 ℃, 50 MPa) using ZnF_2 as an additive [7]. Maxim produced ZA ceramic by SPS using LiF as an additive [8]. Xu also fabricated fully dense ZA ceramic via SPS by incorporating tetraethyl orthosilicate (TEOS) [10].

Furthermore, due to the similarity between ZA ceramic and MA ceramic, zinc oxide can be used as an additive to improve the properties of MA ceramic [11]. Ghosh discovered that the optimum properties of MA, including bulk density, hot strength and thermal shock resistance, were obtained on being sintered at 1550 ℃ with the addition of 1 wt.% ZnO [12]. Wang found that ZnO addition could significantly increase the amount of MA spinel through the creation of solid solution $(Mg_xZn_{1-x})Al_2O_4$, which greatly improved the densification and flexural strength of the material [13]. Therefore, the addition of MgO should have a similar effect on the preparation and properties of ZA ceramic, although few studies have been reported on this topic.

In this work, ZA ceramic was prepared from Al_2O_3 and ZnO by solid-state reaction sintering using MgO as an additive. The effect of MgO addition on the micro-structure and mechanical properties of ZA ceramic was investigated in detail and the strengthening mechanism of MgO addition was revealed.

2. EXPERIMENTAL

The used raw materials were analytically pure alumina (Al_2O_3) and zinc oxide (ZnO) from Sinopharm Chemical Reagent Co. Ltd and analytically pure magnesia (MgO) was used as an additive from Tianjin Zhiyuan Chemical Reagent Co. Ltd.

Al_2O_3 and ZnO were mixed according to the theoretical molar ratio of 1:1, and MgO was added according to the mass percentage of the mixed powder, namely 0.5 %, 1.0 %,

* Corresponding author: J. Hao
E-mail: *jianyinghao@tyust.edu.cn*

1.5 %, 2.0 %, 2.5 %, 3.0 %, 3.5 %, marked as Q1, Q2, Q3, Q4, Q5, Q6 and Q7 in turn. The specimen without MgO addition was designated as Q0. All raw materials were initially mixed and wet-milled for 4 h in a planetary ball mill (LGB04, Nanjing Boyuntong Instrument Technology Co. Ltd, China) with the medium of deionized water. Subsequently, the resulting slurry was dried in a drying oven (DH-101-2BS, Tianjing Central Experimental Furnace Co. Ltd, China) at 80 ℃ for 24 h. And then, the powder was compressed into cuboid sample approximately 30 mm × 6 mm × 6 mm under pressure of 20 MPa. Finally, the pressed sample was sintered in a high temperature box sintering furnace (KBF1700, Nanjing Boyuntong Instrument Technology Co. Ltd, China) at 1200 ℃, 1300 ℃, 1400 ℃, 1500 ℃, 1600 ℃ for 3 h at heating rate of 5 ℃/min, and then, cooled with the furnace.

The phase composition of the sample was analyzed by X-ray powder diffraction (XRD, X'Pert PR, Philips Co. Ltd, Netherlands) with the scanning speed of 4°/min. The microstructure of the sample was observed by field emission scanning electron microscopy (SEM; S-4800, Hitachi, Japan) at an accelerating voltage of 20 kV.

According to Archimedes' principle, bulk density (P, g/cm^3) and apparent porosity (D, %) of the sample were measured by Eq. 1 and Eq. 2 [14]:

$$P = (m_1 - m_0)/(m_1 - m_2) \times 100\%; \quad (1)$$

$$D = m_0 D_1/(m_1 - m_2), \quad (2)$$

where m_0 is the dry mass of the sample, g; m_1 is the floating mass of saturated sample in the liquid, g; m_2 is the wet mass of the saturated sample, g; D_1 is the density of water, 1.0 g/cm^3.

Flexural strength (σ, MPa) was tested by flexural strength testing machine (YDW-10, Jinan Hengxu Testing Machine Co., Ltd., China) at speed of 5 N/s. The equation was as follows [14]:

$$\sigma = 3Fl/(2bh^2), \quad (3)$$

where F is the force loaded on the sample, N; l is the span (20.7 mm); b and h are respectively the width and height of the sample, mm and mm.

3. RESULTS AND DISCUSSION

The XRD patterns of the samples with different magnesia content sintered at 1600 ℃ for 3 h are presented in Fig. 1. Obviously, the main crystalline phase of all samples is gahnite ($ZnAl_2O_4$, ZA, PDF: 05-0669) in Fig. 1 a, and all the diffraction peaks are very similar, indicating that the increase of magnesia content does not have a great effect on ZA crystal. In order to investigate the effect of magnesia addition on ZA crystal in more detail, principal crystal planes (220) and (311) are enlarged in Fig. 1 b. It can be seen that the addition of magnesia makes the diffraction peaks shift slightly to the right, revealing that magnesia can dissolve into ZA phase. An interesting phenomenon occurs when individual sample is compared by Jade 6.0. Sample Q4 containing 2 % magnesia begins to show some new diffraction peaks and are detected as zincite (ZnO, PDF:36-1451). Therefore, samples Q4-Q7 with a magnesia content of not less than 2 % are compared, and the results are presented in Fig. 1 c. The diffraction peak intensity of ZnO gradually increases with the increase of magnesia content, indicating that excess ZnO in the precursor does not participate during the sintering process due to the addition of magnesia.

Sardelli confirmed the higher reactivity of the Al_2O_3-ZnO system when compared to the Al_2O_3-MgO system [15]. Meanwhile, Yuvaraj suggested that Mg^{2+} was one of the fascinating transition metal with higher thermal stability and easily replaced Zn^{2+} in the sub-lattice of ZA upon adding MgO, and this replacement caused the enhancement in the thermal stability [16]. Furthermore, the ionic radii of Zn^{2+} and Mg^{2+} are similar (0.74Å for Zn^{2+} and 0.71Å for Mg^{2+}), [16] so Mg^{2+} may substitute Zn^{2+} in the ZA, which favors the formation of solid solution ($Mg_xZn_{1-x}Al_2O_4$) [17]. Simultaneously, lattice strain and anion vacancy are generated, which enhances the ions movement and mass transfer [16].

To further illustrate the effect of magnesia addition on ZA crystals, the full width at half maximum (FWHM) values of main crystal planes (220) and (331) of ZA are obtained by Jade 6.0 and shown in Fig. 1(d). Obviously, the FWHM values slowly decrease with the increase of magnesia content. According to Scherrer's Eq. 4 [18] the FWHM is inversely proportional to the grain size, indicating that the addition of magnesia will increase the grain size of ZA.

$$D = K\lambda/(\beta\cos\theta), \quad (4)$$

where K is the constant (0.90), λ is the X-ray wavelength (0.1540 nm); β is the line broadening at half the maximum intensity; θ is the Bragg angle; D is the crystallite size.

The XRD patterns of sample Q5 sintered at different temperatures are shown in Fig. 2 a.

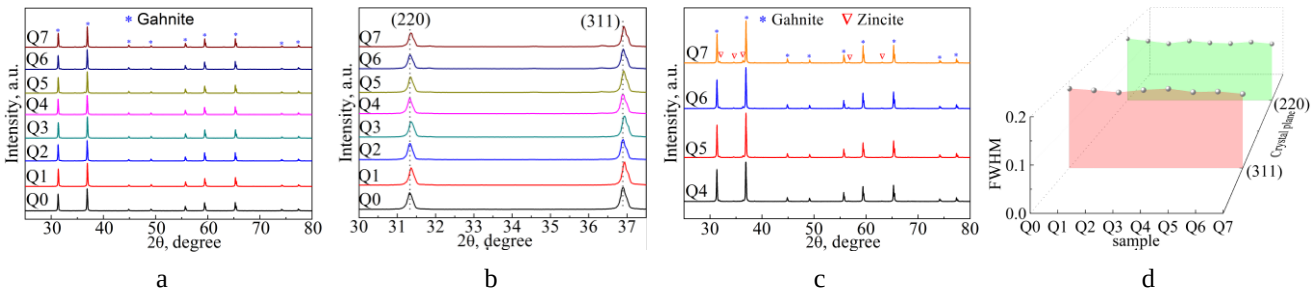

Fig. 1. XRD patterns of the prepared samples with magnesia addition: a – Q0-Q7; b – crystal planes (220) and (311); c – Q4-Q7; d – FWHM of crystal planes (220) and (311)

When the sintering temperature increases from 1200 ℃ to 1600 ℃, the diffraction peak intensity of ZA increases significantly, displaying that the reaction between Al_2O_3 and ZnO is more complete, resulting in higher crystallinity of ZA. The enlargement of XRD patterns the crystal plane (101) of zincite and crystal plane (311) of gahnite is shown in Fig. 2 b. With the increase of temperature, the peak intensity of crystal plane (101) becomes weaker, while that of crystal plane (311) becomes stronger. Jain proposed that ZnO dissolved in ZA lattice accompanied by the formation of oxygen vacancies and zinc interstitial [19]. The decrease of the diffraction peak intensity of ZnO may be related to the solid solution of ZnO to ZA spinel, or to slight volatility or miniscule sublimation of ZnO during calcination [8, 20]. The peak intensity of ZA spinel increases, indicating that high temperature is beneficial to the crystallization of spinel. In addition, the diffraction peak of crystal plane (311) slightly shifts toward lower diffraction angle, which is consistent with the report that Mg^{2+} doped to ZA spinel [16].

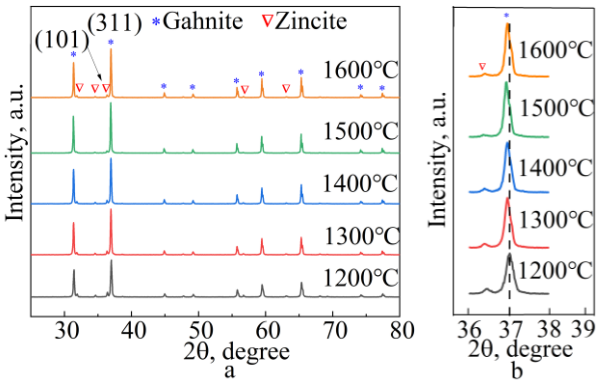

Fig. 2. XRD patterns of sample Q5 sintered: a – at different temperatures; b – crystal planes (101) and (311)

The bulk density and apparent porosity of prepared samples are presented in Fig. 3. Fig. 3 a reflects the density and porosity of the samples with different magnesia content sintered at 1600 ℃. The densification of samples Q0-Q5 is clearly enhanced with increasing magnesia content. Sample Q5 obtains the highest densification (4.1 g/cm^3 of bulk density and 6.01 % of apparent porosity), while the density of sample Q0 is the lowest and its porosity is the highest. When adding magnesia, the density of ZA ceramic sharply increases because the liquid phase produced by the addition of magnesia can promote the sintering of ZA ceramic through the liquid phase sintering mechanism [14]. The addition of magnesia can make Mg^{2+} replace Zn^{2+} to form solid solution $Mg_xZn_{1-x}Al_2O_4$, which may be accompanied by the generation of Zn^{2+} vacancies, significantly enhancing ion diffusion and improving the mass transport process for structural densification [12, 21]. Subsequently, the density of samples Q6 and Q7 decreases as continuing to increase magnesia content. This may be related to the excessive liquid phase produced by magnesia. However, it is worth noting that the bulk density of samples Q6 and Q7 is still higher, 3.9 g/cm^3 and 3.88 g/cm^3 respectively, which is much higher than that of the sample without magnesia addition (3.3 g/cm^3). And the corresponding porosity is also lower, 8.5 % and 9.1 % respectively.

The bulk density and apparent porosity of sample Q5 sintered at different temperatures are presented in Fig. 3 b. When the temperature is raised, the densification of sample Q5 gradually increases and the porosity continuously descends, mainly due to good sintering ability at higher temperature [13]. In short, high temperature is beneficial to the sintering of ZA ceramic, and the addition of magnesia obviously improves the densification of the samples.

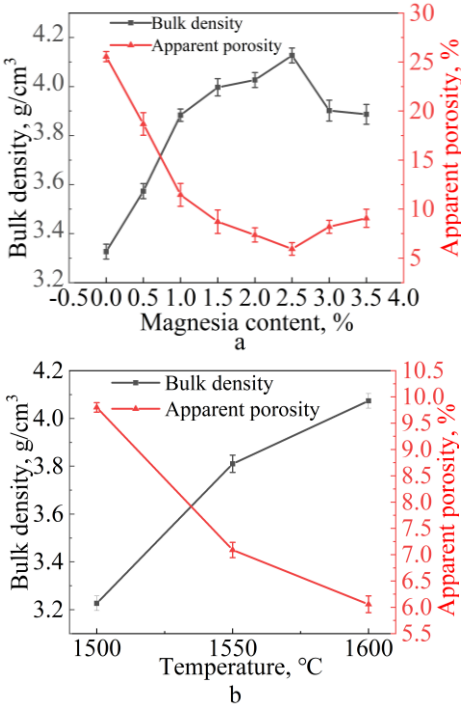

Fig. 3. Bulk density and apparent porosity of the samples: a – adding different amounts of magnesia; b – sintered at different temperatures

The flexural strength of synthetic samples is shown in Fig. 4. Fig. 4 a displays the flexural strength of the samples with different content of magnesia. The strength first rises and then declines with the increase of magnesia content. The variation trend of densification and flexural strength is matched, and the relationship between apparent porosity and flexural strength is depicted in Eq. 5 [13]:

$$\sigma = \sigma_1 e^{-bt}, \quad (5)$$

where σ is the flexural strength; b is the pore structure constant; t is the porosity; σ_1 is the flexural strength under the material's standard bulk density. When the porosity decreases, the flexural strength is enhanced. Sample Q5 exhibits the most considerable flexural strength (198.7 MPa). Subsequently, when 3.0 % and 3.5 % magnesia are added, the flexural strength decreases clearly, 187.9 MPa and 165.7 MPa respectively, much higher than that of $MgAl_2O_4$ spinel (93.5 MPa) [22]. Shen reported that the flexural strength of ZA prepared with bauxite as raw material was up to 177.38 MPa, and that of ZA adding pyrolusite as an additive was increased to 210.61 MPa [23, 24].

The flexural strength of sample Q5 sintered at different temperatures is reflected in Fig. 4 b. The flexural strength of sample Q5 gradually increases with the increase of temperature, which is closely related to the increase of densification. This increase is mainly ascribed to highly dense structure with smaller pore, which is based on the law

that the value of flexural strength increases by an exponential law with decreasing the porosity of ceramic materials [25]. When the temperature rises from 1500 ℃ to 1550 ℃, the flexural strength sharply rises from 170.7 MPa to 191.9 MPa. As the temperature continues to rise to 1600 ℃, the strength increases slowly, reaching 198.7 MPa, indicating that the structure is relatively dense at 1550 ℃. Similarly, the flexural strength is also much higher than that reported in the literatures [13, 25]. The high density and high strength characteristics of sample Q5 can make it used as a preparation scheme for materials with high strength and high refractory properties [26].

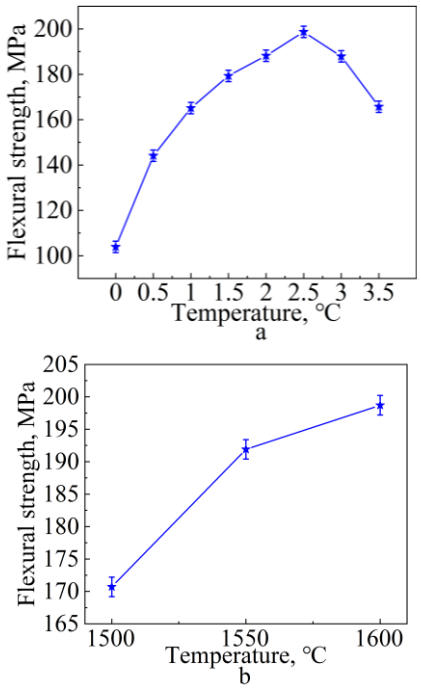

Fig. 4. Flexural strength of the samples: a – adding different amounts of magnesia; b – sintered at different temperatures

SEM images of the samples sintered at 1600 ℃ with different magnesia content are presented in Fig. 5. Increasing magnesia content can induce the continuous growth of ZA crystals, which is consistent with the results in Fig. 1 d. As can be seen from Fig. 5 a, the synthesized ZA crystals are bonded together by bottleneck action. In addition, the pores between the particles are large and interpenetrate, and the particles also have agglomerate phenomenon [26]. The loose structure makes the density and strength of sample Q0 low, which is consistent with the results in Fig. 3 a and Fig. 4 a. In Fig. 5 b, after adding 0.5% magnesia, the ZA grains clearly grow up and particle agglomeration is still present, which may be related to a small amount of liquid phase produced by magnesia. Furthermore, the pores between the particles apparently shrink except for a few large pores and the structure density increases, which may be related to the growth of grains occupying the space of the pores. This also indicates that the addition of magnesia may promote the development and growth of ZA grains. For samples Q2 and Q3 (Fig. 5 c and d), the ZA grains continue to grow, with an average diameter of about 3 μm, and the structure is further compact, displaying that the performance has been improved. Moreover, the large pores disappear significantly, and only a few small pores are left by the accumulation of particles, which is mainly due to the liquid phase produced by magnesia. In Fig. 5 e, the ZA grains still continue to grow and have sharp edges, with an average diameter of about 5 μm. In addition, the structure remains dense, but small pores still appear. As 2.5 % magnesia is added (Fig. 5 f), the ZA grains are well developed and show an obvious structure, and the crystal grains are closely arranged, resulting in an obvious reduction of small pores. Moreover, the grain boundaries are very clear, showing that sufficient liquid phase promotes the development and growth of ZA grains. At this time, Mg^{2+} replaces Zn^{2+} to form the solid solution $(Mg_xZn_{1-x})Al_2O_4$, reducing the lattice disorder and increasing the density of ZA ceramic. In Fig. 5 g and h, as more magnesia is further added, some ZA grains continue to grow, and even abnormal growth of the grains appears, especially as shown in Fig. 5 h. This phenomenon may be related to excessive liquid phase produced by excessive magnesia. It is worth noting that the formation of ZA grains is the accumulation of crystal nuclei by layers. In conclusion, it is clearly revealed from Fig. 5 that the addition of magnesia contributes to the crystallization and growth of ZA crystals, and improves the densification of the structure.

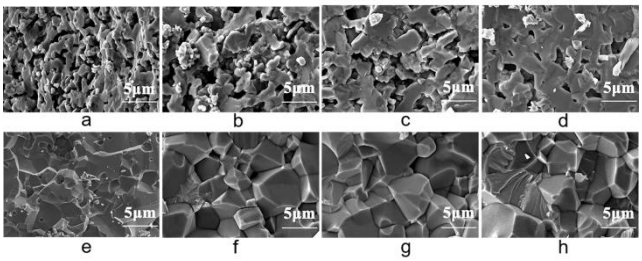

Fig. 5. SEM images of the samples with different amounts of magnesia: a – Q0; b – Q1; c – Q2; d – Q3; e – Q4; f – Q5; g – Q6; h – Q7

SEM images of sample Q5 sintered at 1500 – 1600 ℃ are shown in Fig. 6. In Fig. 6 a, the ZA grains are well developed, and their edges are clearly visible when sample Q5 is sintered at 1500 ℃. These grains are tightly packed, and there are some pores at the intersection of the grains. When the sintering temperature increases to 1550 ℃ (Fig. 6 b), the grains significantly grow up, and the structure becomes denser although the pores are still present, which is consistent with the results in Fig. 3 b. And small pores can also appear. As sintered at 1600 ℃, the ZA grains continue to grow, and the pores are obviously reduced, resulting in more dense structure. In addition, the grain has a small dihedral angle of 120°, indicating that the crystals are well developed [21]. In short, the grains develop better and grow with the increase of temperature, which also confirms that the sintering temperature has a great relationship with the crystal crystallization.

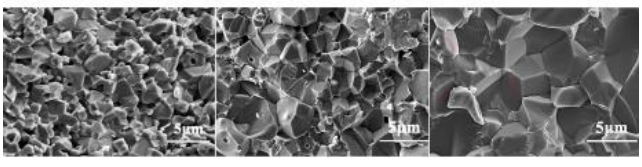

Fig. 6. SEM images of sample Q5 sintered at different temperatures: a – 1500 ℃; b – 1550 ℃; c – 1600 ℃

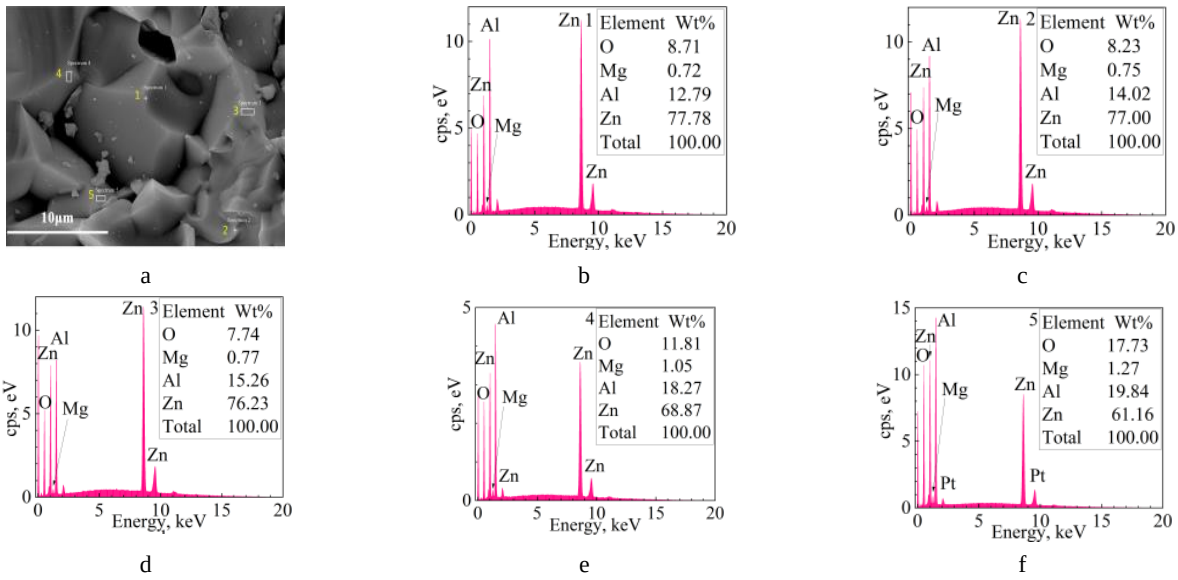

Fig. 7. EDS images in five representative areas of sample Q5: a – SEM image; b, c – points 1 and 2; d, e, f – regions 3 – 5

According to XRD analysis, the content of zincite (ZnO) phase increases with the increase of magnesia, and no other new phase except gahnite and zincite is detected, indicating the formation of uniform solid solution. Fig. 7 depicts the EDS images in five representative areas of sample Q5, and Fig. 8 represents the distribution of elements in the representative region of sample Q5. The EDS and mapping images confirm the existence of elements O, Al, Zn and Mg. It is well-known that Mg^{2+} easily replaces Zn^{2+} in the sublattice of ZA upon doping with Mg^{2+} [16].

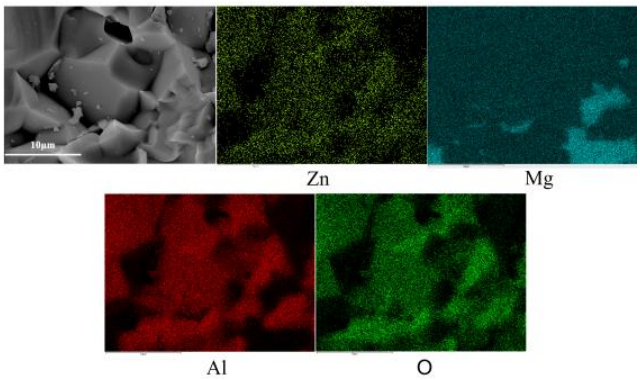

Fig. 8. Distribution of elements in a representative area of sample Q5

This replacement can induce lattice strain and create cation vacancy, which enhances the ions movement and mass transfer [17, 26]. The compositions of two representative points 1 and 2 in Fig. 7 indicate that the content of Mg is respectively 0.72 % and 0.75 %, while the content of Zn is respectively 77.78 % and 77.00 %, displaying that the content of elements in the gaps or pores on the crystal surface is very similar. The content of Mg in the crystals of small regions 3, 4 and 5 is slightly larger than that of points 1 and 2, which is mainly related to the size of the selected region. Meanwhile, the content of Zn is relatively reduced, but the difference is not very large. This also indicates that the distribution of Mg is relatively uniform. Moreover, the results in Fig. 5 also reveal that the Mg^{2+} addition does promote the growth of ZA grains, even over growth. However, the distribution of Mg in Fig. 8 is slightly different. It can be seen in Fig. 8 that Mg is mainly concentrated in the lower-right corner region, displaying that the diffusion of Mg^{2+} is hindered. The presence of free Zn^{2+}, substituted by Mg^{2+}, can hinder the grain boundary migration and the ions diffusion as the second phase [21]. It is also worth noting that where Mg is concentrated, the grain size is smaller and the structure is denser, which makes the properties better.

In brief, the replacement of Mg^{2+} for Zn^{2+} can induce lattice strain and generate cation vacancy, which reduces the activation energy for ion migration, significantly enhancing the ion diffusion and improving the mass transport process for densification. On the other hand, free Zn^{2+} replaced by Mg^{2+} as the second phase (zincite) can hinder grain boundary migration and refine grains, thus improving the properties. The distribution of Mg^{2+} in the crystals is the comprehensive effect of the cation vacancy resulting from the substitution reaction and the inhibition of free zinc.

4. CONCLUSIONS

Analytically pure alumina and zinc oxide were used as raw materials to produce $ZnAl_2O_4$ ceramics, and magnesia was selected as an additive to improve its properties. The effects of different magnesia contents and sintering temperature on the densification, sintering process and mechanical properties of $ZnAl_2O_4$ ceramics were studied in detail, and the following conclusions were obtained.

The addition of magnesia can improve the densification and flexural strength of $ZnAl_2O_4$ ceramic with the increase of sintering temperature. $ZnAl_2O_4$ ceramics has the best densification and the highest strength as adding 2.5 % magnesia and sintered at 1600 °C. The bulk density and apparent porosity are respectively 4.1 g/cm^3 and 6.01 %, and the flexural strength is 198.7 MPa, which is much higher than that without magnesia addition (103.9 MPa).

The radius of Mg^{2+} is close to that of Zn^{2+}, therefore Mg^{2+} can easily replace Zn^{2+} to form solid solution Mg_xZn_{1-}

$_xAl_2O_4$ during sintering. The generated solid solution $Mg_xZn_{1-x}Al_2O_4$ can promote the development and growth of $ZnAl_2O_4$ grains, thereby improving the densification of $ZnAl_2O_4$ ceramics. In addition, the substituted zincite as the second phase can prevent grain boundary migration and locally refine grains, resulting in the improvement of the performance.

Acknowledgments

This work was supported by the Basic Research Project of Shanxi Province [grant number 202203021211186]; Taiyuan University of Science and Technology Doctoral Start-up Fund Project [grant number 20212028].

REFERENCES

1. **Lotfian, N., Nourbakhsh, A.A., Mirsattari, S.N., Mackenzie, K.J.D.** Functionalization of Nano-$MgCr_2O_4$ Additives by Silanol Groups: A New Approach to the Development of Magnesia-chrome Refractories *Ceramics International* 47 (22) 2021: pp. 31724 – 31731. https://doi.org/10.1016/j.ceramint.2021.08.052
2. **Baudin, C., Martinez, R., Pena, P.** High-temperature Mechanical Behavior of Stoichiometric Magnesium Spinel *Journal of the American Society* 78 (8) 1995: pp. 1857 – 1862. https://doi.org/10.1111/j.1151-2916.1995.tb08900.x
3. **Li, Y., Guo, L., Chen, L.G., Ding, D.F., Ye, G.T.** Effect of $Zn(OH)_2$ on Properties of Corundum Based Castables Bonded with Calcium Aluminate Cement *Ceramics International* 47 (1) 2021: pp. 57 – 63. https://doi.org/10.1016/j.ceramint.2020.07.102
4. **Ouyang, X., Wu, S.P., Wang, Z.L., Liu, Y.H.** Synthesis and Microwave Dielectric Properties of $2ZnO{\cdot}3B_2O_3$-Doped $ZnAl_2O_4$ Low-permittivity Ceramics *Journal of Alloys and Compounds* 644 2015: pp. 242 – 248. https://doi.org/10.1016/j.jallcom.2015.04.151
5. **Qin, T.Y., Zhong, C.W., Qin, Y., Tang, B., Zhang, S.R.** Low-temperature Sintering Mechanism and Microwave Dielectric Properties of $ZnAl_2O_4$-LMZBS Composites *Journal of Alloys and Compounds* 797 2019: pp. 744 – 753. https://doi.org/10.1016/j.jallcom.2019.05.141
6. **Van der Laag, N.J., Snel, M.D., Magusin, P.C.M.M., De With, G.** Structural, Elastic, Thermophysical and Dielectric Properties of Zinc Aluminate ($ZnAl_2O_4$) *Journal of the European Ceramic Society* 24 (8) 2004: pp. 2417 – 2424. https://doi.org/10.1016/j.jeurceramsoc.2003.06.001
7. **Belyaev, A.V., Evdokimov, I.I., Drpbptenko, V.V., Sorokin, V.V.** A New Approach to Producing Transparent $ZnAl_2O_4$ Ceramics *Journal of the European Ceramic Society* 37 (7) 2017: pp. 2747 – 2751. https://doi.org/10.1016/j.jeurceramsoc.2017.02.041
8. **Maxium, S., Shay, M., Einat, S., Sergey, K., Shmuel, H.Y., Nachum, F.** On the Effects of LiF on the Synthesis and Reactive Sintering of Gahnite ($ZnAl_2O_4$) *Ceramics International* 43 (17) 2017: pp. 14891 – 14896. https://doi.org/10.1016/j.ceramint..2017.08.005
9. **Chassagne, J., Petit Meunier, C., Valdivieso, F.** Preparation of Magnesium and Zinc Aluminate Spinels by Microwave Heating: Influence of the Oxide Precursors on the Phase Composition *Materials Today Communication* 33 2022: pp. 104679. https://doi.org/10.1016/j.mtcomm.2022.104679
10. **Xu, Y., Fu, P., Zhang, B.H., Gao, J., Zhang, L., Wang, X.H.** Optical Properties of Transparent $ZnAl_2O_4$ Ceramics: A New Transparent Material Prepared by Spark Plasma Sintering *Materials Letters* 123 2014: pp. 142 – 144. https://doi.org/10.1016/j.matlet.2014.03.013
11. **Zheng, C.W., Wu, S.Y., Chen, X.M., Song, K.X.** Modification of $MgAl_2O_4$ Microwave Dielectric Ceramics by Zn Substitution *Journal of the American Ceramic Society* 90 (5) 2007: pp. 1483 – 1486. https://doi.org/10.1111/j.1551-2916.2007.01550.x
12. **Ghosh, A., Das, S.K., Biswas, J.R., Tripathi, H.S., Banerjee, G.** The Effect of ZnO Addition on the Densification and Properties of Magnesium Aluminate Spinel *Ceramics International* 26 (6) 2000: pp. 605 – 608. https://doi.org/10.1016/S0272-842(99)00104-2
13. **Wang, X.J., Tian, Y.M., Hao, J.Y., Wang, Y.Y., Bai, P.B.** Sintering Mechanism and Properties of $MgAl_2O_4$-$CaAl_{12}O_{19}$ Composites with ZnO Addition *Journal of the European Ceramic Society* 40 (15) 2020: pp. 6149 – 6154. https://doi.org/10.1016/j.jeurceramsoc.2020.07.008
14. **Xuan, S.T., Tian, Y.M., Kong, X.C., Hao, J.Y., Wang, X.J.** Effect of Different MgO/Al_2O_3 Ratios on Microstructural Densification, Sintering Process and Mechanical Property of $MgAl_2O_4$ Materials *Journal of Materials Research Technolgy* 25 2023: pp. 2518 – 2526. https://doi.org/10.1016/j.jmrt.2023.06.044
15. **Sardelli, J.A.P., Borges, O.H., Pagliosa Neto, C., Pandolfelli, V.C.** Is the In-situ $ZnAl_2O_4$ Formation An Alternative for Magnesia-alumina Spinel Zero-carbon Shaped Refractories? *Ceramics International* 49 (17) 2023: pp. 28643 – 28650. https://doi.org/10.1016/j.ceramint.2023.06.119
16. **Yuvaraj, S., Ramachandran, S., Subramani, A., Thamilselvan, A., Venkatesan, S., Sundararajan, M., Dash, C.S.** Impact of Mg^{2+} Ion on the Structural, Morphological, Optical, Vibrational, and Magnetic Behavior of Mg:$ZnAl_2O_4$ Spinel *Journal of Superconductivity and Novel Magnetism* 33 (4) 2020: pp. 1199 – 1206. https://doi.org/10.1007/s10948-019-05347-7
17. **Mandal, S., Hemrick, J.G., Mahapatra, M.K.** Impact on Aggregate/Matrix Bonding When A Refractory Contains Zinc Aluminate Instead of Spinel and Magnesia-chrome *Journal of the American Ceramic Society* 106 (10) 2023: pp. 5662 – 5678. https://doi.org/10.1111/JACE.19214
18. **Boyraz, C., Seker Perez, M.M., Arda, L.** Structure, Microstructure, and ESR Properties of Concentration-dependent $Zn_{1-x}Mn_xO$ Nanoparticles *Ceramics International* 50 (23) 2024: pp. 50855 – 50866. https://doi.org/10.1016/j.ceramint.2024.09.432
19. **Jain, M., Manju, N., Gundimeda, A., Thakur, A.** Defect Induced Broadband Visible to Near-infrared Luminescence in $ZnAl_2O_4$ Nanocrystals *Applied Surface Science* 480 2019: pp. 945 – 950. https://doi.org/10.1016/j.apsusc.2019.02.198
20. **Xu, P., Wang, H., Ren, L., Tu, W., Wang, W., Fu, W.** Theoretical Study on Composition Dependent Properties of $ZnO{\cdot}nAl_2O_3$ Spinels. Part I: Optical and Dielectric *Journal of the American Ceramic Society* 104 (10) 2021: pp. 5099 – 5109. https://doi.org/10.1111/JACE.17756
21. **Mohapatra, D., Sarkar, D.** Preparation of MgO-$MgAl_2O_4$ Composite for Refractory Application *Journal of Materials Processing Technology* 189 (1 – 3) 2007: pp. 279 – 283.

https://doi.org/10.1016/j.jmatprotec.2007.01.037

22. **Zhou, Y., Ye, D.C., Wu, Y.Q.** Low-cost Preparation and Characterization of $MgAl_2O_4$ Ceramics *Ceramics International* 48 (5) 2022: pp. 7316 – 7319. https://doi.org/10.1016/j.ceramint.2021.11.196
23. **Shen, Q.K., Hao, J.Y., Zhu, Z.G., Bai, S.** Preparation and Performance Optimization of Zinc Aluminate Ceramic by Solid-state Reaction Sintering *Ceramics International* 20 (50) 2024: pp. 39574 – 39580. https://doi.org/10.1016/j.ceramint.2024.07.336
24. **Shen, Q.K., Hao, J.Y., Zhu, Z.G., Bai, S.** Optimization of Compactness and Mechanical Properties of Zinc Aluminate Ceramics under the Synergistic Control of Pyrolusite Doping and Sitering Temperature *Ceramics International* 51 (6) 2025: pp. 8107 – 8115. https://doi.org/10.1016/j.ceramint.2024.12.246
25. **Xuan, S.T., Tian, Y.M., Kong, X.C., Hao, J.Y., Wang, X.J.** Enhancement of Thermal Shock Resistance of Al_2O_3-$MgAl_2O_4$ Composites by Controlling the Content and Distribution of Spinel Phase *Ceramics International* 49 (24) 2023: pp. 39908 – 39916. https://doi.org/10.1016/j.ceramint.2023.09.256
26. **Xu, L., Chen, M., Yin, X., Wang, N., Liu, L.** Effect of TiO_2 Addition on the Sintering Densification and Mechanical Properties of $MgAl_2O_4$-$CaAl_4O_7$-$CaAl_{12}O_{19}$ Composite *Ceramics International* 42 (8) 2016: pp. 9844 – 9850. https://doi.org/10.1016/j.ceramint.2016.03.082